Nanophotonic luminescent solar concentrators

I. Rousseau and V. Wood[a)]
Laboratory for Nanoelectronics, Department of Information Technology and Electrical Engineering, ETH Zurich, Gloriastrasse 35, CH-8092 Zurich, Switzerland

(Received 5 July 2013; accepted 9 September 2013; published online 27 September 2013)

We investigate the connection between photonic local density of states and luminescent solar concentrator (LSC) performance in two manufacturable nanocavity LSC structures: a bilayer slab and a slab photonic crystal. Finite-difference time-domain electromagnetic simulations show that the waveguided luminescence photon flux can be enhanced up to 30% for the photonic crystal design over a conventional LSC operating in the ray optic limit, assuming the same number of excited lumophores. Further photonic engineering could realize an increase of up to one order of magnitude in the flux of waveguided luminescence. © *2013 AIP Publishing LLC*.
[http://dx.doi.org/10.1063/1.4823538]

The luminescent solar concentrator (LSC) could decrease the installed cost of solar energy through building integration.[1] The LSC, a semi-transparent waveguide with embedded lumophores, concentrates sunlight by frequency downconversion: The lumophores absorb diffuse incident sunlight and luminesce at a redder, Stokes-shifted wavelength. The majority of the luminescence is emitted into modes that can be guided by total internal reflection (TIR) to the waveguide edges, upon which small-area, high efficiency solar cells are fastened.

Despite the LSC's simplicity, the concept has not been commercialized due to low performance. Experimental realizations have demonstrated a twelve-fold concentration of solar flux[2] and power conversion efficiency of 7.2%, well below the theoretical predictions of a flux concentration in excess of 100 (Ref. 3) and power conversion efficiency of 26.8%.[4] Reabsorption of luminescence and subsequent re-emission into non-waveguided modes has been identified as the primary performance bottleneck.[5–9]

While prior work has demonstrated that LSCs consisting of lumophores embedded in optical nanocavities exhibit enhanced waveguiding[10] and reduced reabsorption,[11] the nanocavity modifies the photonic local density of states (LDOS) and therefore the spatial and temporal luminescence distributions.[12,13] Here, we investigate the effect of the modified LDOS on LSC performance using first-principles simulations of Maxwell's equations in two realistic nanocavity LSC designs (Fig. 1, insets). After establishing a link between photonic LDOS and LSC performance, we use finite-difference time-domain (FDTD) simulations to show that a nanocavity LSC can increase the flux of waveguided luminescence photons by up to 30% over a conventional LSC. Finally, we assess the maximum theoretical performance gains from LDOS engineering in the LSC.

First, we define a metric of LSC performance, connect the performance metric to the photonic LDOS, and determine the conditions under which LSC performance comparisons can be made on the basis of the photonic LDOS. Luminescence photons are spontaneously emitted into one of many photonic modes of the LSC. These can be divided into two groups based on the wavevector in the LSC plane ($\mathbf{k}_\parallel$): non-waveguided ($\omega \geq c|\mathbf{k}_\parallel|$) and total internally reflected (TIR, $\omega < c|\mathbf{k}_\parallel|$) modes. In conventional LSCs, lumophore-filled waveguides of refractive index n much thicker than the luminescence wavelength, the fraction $f_{tir} = \sqrt{n^2-1}/n$ of photonic modes corresponds to TIR modes.[1] According to ray tracing simulations, photons emitted into non-waveguided modes are lost into air after multiple reflections.[5] Thus, our analysis assumes that only luminescence photons emitted into TIR modes can be collected by the solar cells attached to the LSC edges.

Assuming the lumophore has unity quantum yield and the LSC surfaces are smooth, a photon emitted into a TIR mode can either be reabsorbed by the lumophore or absorbed by the solar cells affixed to the LSC edges.[4,14] Starting from the quantum optical master equation for a single, lossy photonic mode weakly coupled to a lumophore, we derive a recursion relation for the occupation probability (ρ_n) of a n-photon Fock state[15]

$$\begin{aligned}\dot{\rho}_n = {} & A_{\omega k} n \rho_{n-1} - A_{\omega k}(n+1)\rho_n - B_{\omega k} n \rho_n \\ & - D_{\omega k} n \rho_n + (n+1)(B_{\omega k} + D_{\omega k})\rho_{n+1}. \end{aligned} \quad (1)$$

Here, $A_{\omega k}$ and $B_{\omega k}$ are the photon emission and absorption rates from Fermi's Golden Rule,[16] and $D_{\omega k}$ is the rate at which photons leak out of the photonic mode.[17] In the case of the LSC, we assume this is the rate at which the luminescence photons are collected by solar cells affixed to the LSC edges.

The solution to Eq. (1) is a geometric series,[15] and the steady-state rate at which photons are collected by the attached solar cells from a single TIR mode is

$$D_{\omega k}\bar{n} = D_{\omega k}\sum_n n\bar{\rho}_n = \frac{A_{\omega k} D_{\omega k}}{B_{\omega k} - A_{\omega k} + D_{\omega k}}. \quad (2)$$

Equation (2) contains the emission rate divided by the sum of the reabsorption and collection rates minus the emission rate. If photons are extracted by the solar cells much faster than they can be reabsorbed ($D_{\omega k} \gg B_{\omega k}$), then Eq. (2) can be further simplified such that the photon collection rate for a single mode is then equal to the emission rate, $D_{\omega k}\bar{n}_{\omega k} = A_{\omega k}$.

[a)]Electronic mail: vwood@ethz.ch

Experimentally, this regime corresponds to either small LSCs or LSCs containing lumophores with small reabsorption, which has been demonstrated by exploiting Förster resonant energy transfer or intersystem crossing.[2] Equation (2) must be summed over all wavevectors corresponding to TIR modes ($|\mathbf{k}_{\|}| > \omega/c$) to find the total flux collected by attached solar cells at each frequency. In this operation regime, LSCs with the same species and number of excited lumophores can be directly compared on the basis of TIR LDOS.[15] Here, we compare TIR LDOS in different LSC designs: a "conventional" LSC comprised of lumophores dispersed in a thick dielectric waveguide and two different nanophotonic LSCs with lumophores embedded in a nanocavity.

In each of the investigated nanophotonic LSC designs, a nanocavity is formed by a high refractive index ($n = 1.7$) lumophore-filled organic material of thickness d, sandwiched between two lower refractive index materials: air ($n = 1$) and a fluoropolymer cladding ($n = 1.3$) of thickness h. Since the fluoropolymer is less than a wavelength thick, luminescence in the nanocavity can leak into the underlying substrate waveguide, which losslessly transports the luminescence to the solar cells attached to its side walls.[11] Provided that the leakage rate $D_{\omega k}$ is much greater than the reabsorption rate $B_{\omega k}$ (Eq. (2)), luminescence is not reabsorbed in the nanocavity. In the bilayer slab LSC (Fig. 1(a), inset), a $n = 1.7$ flint glass substrate is necessary to enable leakage of luminescence into the substrate.[11] The second design, a slab photonic crystal (PC) LSC (Fig. 1(b), inset), further confines the light through the addition of air holes of radius r in a square lattice with lattice constant a, patterned through both the organic and fluoropolymer films. Since the air holes decrease the organic's average refractive index, the substrate-waveguide refractive index can be reduced to that of crown glass ($n = 1.5$), which would lower material costs.

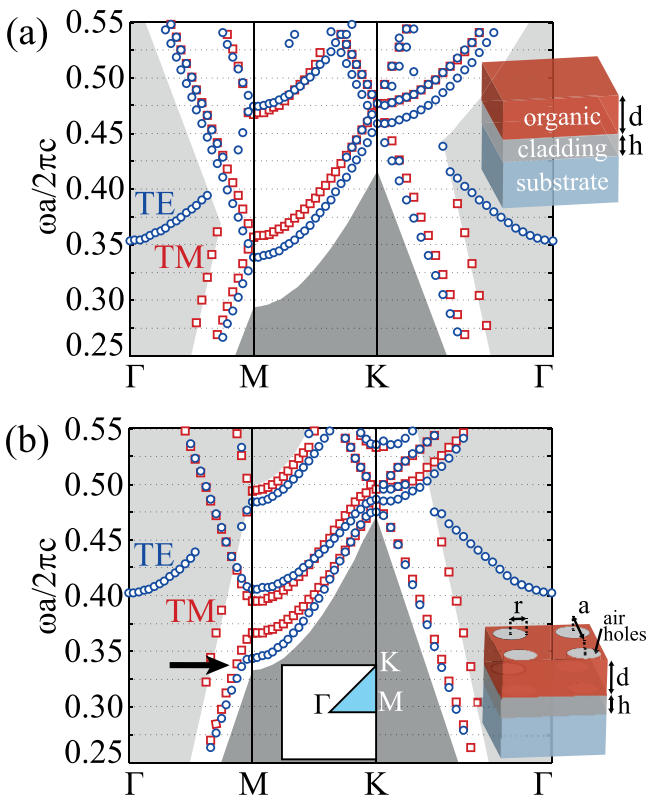

FIG. 1. The band structures for the (a) bilayer slab and (b) slab photonic crystal LSCs. Blue circles represent TE-like modes and red squares, TM-like modes. The light gray corresponds to modes that can leak into both air and the substrate, the white region to generalized TIR modes that can only leak in the substrate, and the dark gray to modes that are confined to the organic. The discrete periodicity of the PC-LSC lifts the degeneracies at the M-point, as indicated by the black arrow.

The photonic LDOS for each three-dimensional structure is computed using a freely available finite-difference time-domain (FDTD) software package.[18] The FDTD method is chosen because the LDOS can be calculated over a broad frequency range in a single simulation.[19] To simulate an infinite periodic photonic crystal, Bloch periodic boundary conditions in the in-plane directions and absorbing boundary conditions in the vertical directions are selected. In order to calculate the LDOS, the electric field transient is recorded at a point after excitation by a point broadband Gaussian current source ($\mathbf{p}(\mathbf{r}, \omega)$) at that same location. The Fourier transform of the electric field transient normalized by the excitation pulse spectrum yields the photonic local density of states for a given location and source orientation[20]

$$\mathrm{LDOS}(\omega, \mathbf{r}, \mathbf{d}) = -\frac{2}{\pi} n(\mathbf{r})^2 \frac{\mathrm{Re}[\mathbf{E}(\mathbf{r}, \omega) \cdot \mathbf{p}^*(\mathbf{r}, \omega)]}{|\mathbf{p}(\mathbf{r}, \omega)|^2}. \quad (3)$$

LDOS calculations are carried out for 2401 wavevectors in a rectangular mesh spanning the irreducible Brillouin zone of the square lattice. Since the LDOS depends on the dipole location and orientation,[21] the total LDOS is averaged over thirty randomly selected locations within the organic volume and three Cartesian dipole orientations to account for anisotropic lumophore emission. Further details explaining the FDTD simulations, **k**-space integration, and LDOS normalization are found in the supplementary material.[15]

Figure 1 displays the simulated band structures, taken from the local maxima in the LDOS, as a function of in-plane wavevector ($\mathbf{k}_{\|}$) between points of high symmetry, Γ, M, and K. To generalize our findings for different lumophores and enable comparison between the two nanophotonic LSCs, we work with dimensionless units incorporating the lattice constant a of the PC-LSC design. The blue circles and red squares indicate TE-like ($\mathbf{E}, \mathbf{p} \parallel \mathbf{k}_{\|}$) and TM-like ($\mathbf{E}, \mathbf{p} \perp \mathbf{k}_{\|}$) modes, respectively.

The simulated dimensions ($h/a = 0.9$, $d/a = 0.5$, and $r/a = 0.275$), while unoptimized, are selected for the LSC application. For both nanocavity LSC designs, the majority of modes lie in the white region. Luminescence emitted into these modes will be transported by TIR in the substrate to the attached solar cells. Furthermore, the bandstructure shows few resonant modes that could cause luminescence to leak into air (light gray region) or remain trapped in the nanocavity (dark gray region). For example, a TE-like etalon resonance occurs in the light gray region near the Γ-point. However, our choice of d/a has positioned this resonance above the spectral region where the lumophore's photoluminescence spectrum should be located. The lumophore should emit where the LDOS is maximized in the white region. For the PC-LSC design, the LDOS is maximized at a $\omega a/2\pi c = 0.345$, as discussed in the following paragraph.

Figure 2 plots the LDOS of the two nanocavity designs. As a reference, the LDOS are shown for conventional LSCs in

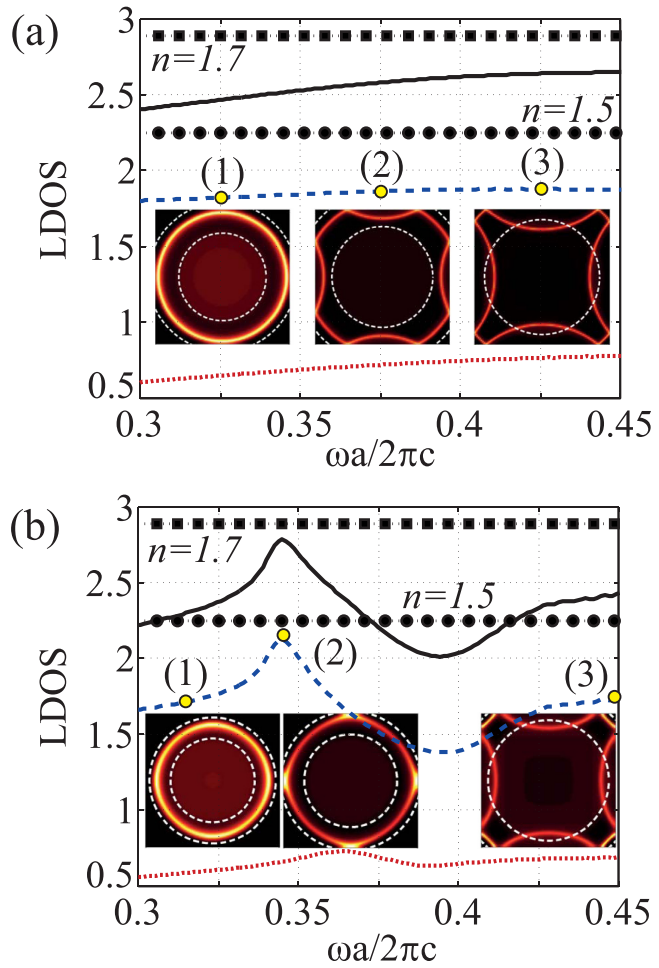

FIG. 2. Total photonic LDOS (black solid lines) for the (a) bilayer LSC and (b) PC-LSC, normalized to the vacuum LDOS. Blue dashed and red dotted lines indicate the contribution of TE-like and TM-like modes to the total LDOS, respectively. Black squares and circles represent the LDOS for $n = 1.7$ and $n = 1.5$ conventional LSCs. Insets show the distributions of spontaneous emission in $\mathbf{k}_{\|}$-space at specific frequencies on a relative scale. Luminescence emitted between the two concentric white dashed circles corresponds to generalized TIR modes in the substrate.

which the lumophores are dispersed in a glass substrate with $n = 1.5$ or $n = 1.7$. To facilitate comparison among the structures, all are normalized to the vacuum LDOS. The bilayer slab (Fig. 2(a)) LDOS is approximately 80% of the $n = 1.7$ conventional LSC, consistent with previous experimental and theoretical work on dielectric slabs.[22] The PC-LSC LDOS (Fig. 2(b)) falls between that of the $n = 1.5$ and $n = 1.7$ conventional LSCs, but does not exceed the $n = 1.7$ conventional LSC.[23] The TE-like (blue) and TM-like (red) contributions to the total LDOS confirm that the LDOS enhancement lies at $\omega a/2\pi c = 0.345$. This enhancement stems from a Van Hove singularity due to the splitting of the photonic bands at the M-point (see black arrow in Fig. 1(b)).[24,25] Finally, the inhibition of the total LDOS between $\omega a/2\pi c = 0.38$ and 0.41 in the PC-LSC means that fewer photons are emitted in the region of strongest overlap between lumophore absorption and luminescence spectra. This feature could potentially be used to mitigate reabsorption.

As expected, the nanocavity LSC spontaneous emission distributions are highly directional (Fig. 2 insets), which is desirable for managing reabsorption losses in the large LSC limit.[11] Luminescence emitted between the two concentric

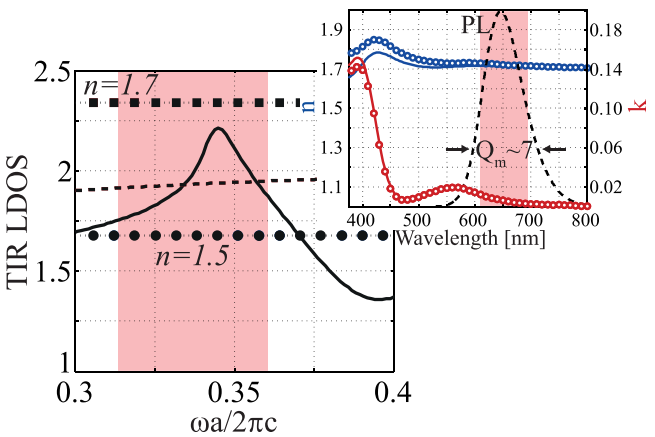

FIG. 3. LDOS corresponding to TIR modes in the PC-LSC (solid line) and bilayer LSC (dashed line) normalized to the total vacuum LDOS. The black squares and circles indicate the TIR LDOS for $n = 1.5$ and $n = 1.7$ conventional LSCs. The inset shows the experimental complex refractive index ($\tilde{n} = n + ik$) and photoluminescence spectrum (black dashed line) of a Alq_3:DCM_2 thin film.[15] The pink shading delineates the FWHM of the photoluminescence spectrum for a specific lattice constant, $a = 222$ nm.

circles is waveguided by generalized TIR (Fig. 1, white region). In both nanocavity LSC designs, a ring corresponding to a single guided TE mode increases in size with frequency and is eventually folded about the band edges due to the Bloch periodic boundary conditions. Since the bilayer LSC has continuous translational symmetry, the folding has no bearing on LSC performance. The folding in the PC-LSC, on the other hand, begins to decrease the TIR LDOS starting at $\omega a/2\pi c = 0.42$, where the second band starts to leak into air (transition from white to gray regions in Fig. 1(b)).

By integrating these partial LDOS distributions between the two light lines, we compute the TIR LDOS for each structure. Fig. 3 compares the TIR LDOS for the nanocavity LSCs with those of conventional LSCs with the same substrate refractive index. The bilayer LSC's TIR LDOS is 15% less than that of the $n = 1.7$ reference. The PC-LSC TIR LDOS exceeds that of a conventional LSC with $n = 1.5$ by up to 31% at the M-point.

To provide a material-specific example, we select a prototypical LSC lumophore system (Fig. 3, inset), the organic laser dye DCM_2 doped into the small molecule organic semiconductor Alq_3.[2,11] The lattice constant $a = 222$ nm maximizes the product of the TIR LDOS with the Alq_3:DCM_2 photoluminescence spectrum (inset) when integrated over the luminescence photon frequency. For this choice of a (pink squares), the PC-LSC demonstrates a modest 10% increase in the TIR luminescent photon flux over the $n = 1.5$ conventional LSC.

In the DCM_2:Alq_3 example, reabsorption of photoluminescence in the nanocavity is minimal. The outcoupling rate $D_{\omega k}$ can be estimated from the FDTD simulations. The quality factor describing luminescence leakage from the nanocavity into the substrate waveguide, $Q_d = \omega/2D_{\omega k}$, is approximately 30 in both designs for the selected dimensions over the photoluminescence spectrum. The reabsorption rate $B_{\omega k}$ can be estimated from electromagnetic perturbation theory,[26] $Q_b = \omega/2B_{\omega k} \approx 170$ for an imaginary refractive index of 0.01 at the photoluminescence peak. Inserting these values into Eq. (2) reveals that roughly 85%

of the luminescence leaks into the substrate waveguide, where it can be nearly losslessly transported to the attached solar cells via resonance shifting.[11]

The maximum TIR LDOS enhancement of spontaneous emission is limited by lumophore photoluminescence spectrum linewidth ($Q_m = \omega_0/\Delta\omega$) to $Q_m/4f_{tir}$.[23] For organics, $Q_m \leq 7$, but Q_m could be up to thirty for state-of-the-art colloidal semiconductor quantum dots.[27] Therefore, if such quantum dots were used in a nanophotonic LSC, the maximum TIR LDOS enhancement would be approximately ten.

In conclusion, we calculated the detailed spatial and spectral luminescence distributions for two nanophotonic LSC designs, which are chosen based on past work as well as manufacturability considerations.[28] Although the directional luminescence distributions are desirable for minimizing reabsorption losses,[11] both the total and TIR spontaneous emission rates are less than the bulk rate for the organic material. By patterning the organic into a photonic crystal, we find that the spontaneous emission rate into TIR modes of the bulk material can be recovered by utilizing dielectric band edge emission in the photonic crystal. The inhibition of the total spontaneous emission rate in a photonic crystal could be further exploited to reduce reabsorption losses in the large LSC limit.

This research was supported by the Swiss National Science Foundation through the National Centre of Competence in Research Quantum Science and Technology and by ETH Research Grant No. ETH-42 12-2. The authors would like to thank the Computational Optics group at ETH and Deniz Bozyigit for helpful discussions.

[1]M. Debije and P. Verbunt, Adv. Energy Mater. **2**, 12–35 (2012).
[2]M. Currie, J. Mapel, T. Heidel, S. Goffri, and M. Baldo, Science **321**, 226–228 (2008).
[3]G. Smestad, H. Ries, R. Winston, and E. Yablonovitch, Sol. Energy Mater. **21**, 99–111 (1990).
[4]T. Markvart, J. Appl. Phys. **99**, 026101 (2006).
[5]J. Batchelder, A. Zewail, and T. Cole, Appl. Opt. **18**, 3090–3110 (1979).
[6]M. Debije, P. Verbunt, B. Rowan, B. Richards, and T. Hoeks, Appl. Opt. **47**, 6763–6768 (2008).
[7]R. Olson, R. Loring, and M. Fayer, Appl. Opt. **20**, 2934–2940 (1981).
[8]W. Weber and J. Lambe, Appl. Opt. **15**, 2299–2300 (1976).
[9]L. Wilson, B. Rowan, N. Robertson, O. Moudam, A. Jones, and B. Richards, Appl. Opt. **49**, 1651–1661 (2010).
[10]J. Gutmann, M. Peters, B. Bläsi, M. Hermle, H. Zappe, and J. Goldschmidt, Opt. Express **20**, A157–A167 (2012).
[11]N. Giebink, G. Wiederrecht, and M. Wasielewski, Nature Photon. **5**, 694–701 (2011).
[12]S. John, Phys. Rev. Lett. **58**, 2486–2489 (1987).
[13]E. Yablonovitch, Phys. Rev. Lett. **58**, 2059–2062 (1987).
[14]E. Yablonovitch, J. Opt. Soc. Am. **70**, 1362–1363 (1980).
[15]See supplementary material at http://dx.doi.org/10.1063/1.4823538 for details on calculations and FDTD simulations.
[16]N. Abraham and S. Smith, Phys. Rev. A **15**, 421–428 (1977).
[17]H. Breuer and F. Petruccione, *The Theory of Open Quantum Systems* (Oxford University Press, Oxford, UK, 2007), pp. 161–162.
[18]A. Oskooi, D. Roundy, M. Ibanescu, P. Bermel, J. Joannopoulos, and S. Johnson, Comput. Phys. Commun. **181**, 687–702 (2010).
[19]A. Koenderink, M. Kafesaki, C. Soukoulis, and V. Sandoghdar, J. Opt. Soc. Am. B **23**, 1196–1206 (2006).
[20]A. Oskooi and S. Johnson, *Advances in Computational Electrodynamics: Photonics and Nanotechnology* (Artech House, Norwood, MA, 2013), p. 7477.
[21]R. Lee, Y. Xu, and A. Yariv, J. Opt. Soc. Am. B **17**, 1438–1442 (2000).
[22]H. Urbach and G. Rikken, Phys. Rev. A **57**, 3913–3930 (1998).
[23]M. Boroditsky, R. Vrijen, T. Krauss, R. Coccioli, R. Bhat, and E. Yablonovitch, J. Lightwave Technol. **17**, 2096–2112 (1999).
[24]K. Busch and S. John, Phys. Rev. E **58**, 3896–3908 (1998).
[25]J. Joannopoulos, S. Johnson, J. Winn, and R. Meade, *Photonic Crystals: Modeling the Flow of Light* (Princeton University Press, Princeton, NJ, 2008), pp. 244–247.
[26]S. Johnson, M. Ibanescu, M. Skorobogatiy, O. Weisberg, J. Joannopoulos, and Y. Fink, Phys. Rev. E **65**, 066611 (2002).
[27]O. Chen, J. Zhao, V. Chauhan, J. Cui, C. Wong, D. Harris, H. Wei, H. Han, D. Fukumura, R. Jain, and M. Bawendi, Nature Mater. **12**, 445–451 (2013).
[28]A. Yokoo, H. Suzuki, and M. Notomi, in *Proceedings of the Microprocesses and Nanotechnology Conference* (2003), pp. 54–55.